XGEO Collection Methods Using New Satellite Observing Techniques on the James Webb Space Telescope

Kaitlyn Raub
The MITRE Corporation
Tim McLaughlin
Pine Park Engineering Corporation
Roger L. Mansfield
Astronomical Data Service

ABSTRACT

We present Pine Park Engineering and MITRE's collection campaign on the James Webb Space Telescope (JWST) during its deployment beyond geosynchronous orbit, or to XGEO space. Included in this paper are the end-to-end collection methods using new satellite observation techniques, an analytical study in the data quality and products, and the challenges presented during the campaign. We will outline the XGEO collection methods that were used in the campaign, address the current challenges that traditional ground-based optical sensors face with these orbits, and outline additional work needed to be fully prepared for the future of XGEO data collection.

The Artemis program, which will return humans to the lunar surface for the first time since Apollo 17, and the recent deployment of NASA's James Webb Space Telescope to beyond the Moon, are just two examples of missions to send spacecraft to XGEO. Traditional methods for satellite observations are rendered unusable for objects near the moon. Common tracking methods are not valid for a 3-body system because of lunar and solar gravitational perturbations, such as those using two-line element sets (TLE's) and standard state vector propagation models. Due to the increasing number of XGEO missions, it is important to identify the limitations of our current tracking and observation capabilities and to establish new ones.

1. INTRODUCTION

Cislunar is defined as the volume of space beyond geosynchronous orbit (GEO) but still contained within the Moon's orbit [1]. XGEO objects are subject to gravitational effects from the Moon and the Earth unlike objects in low Earth orbit (LEO) or GEO, where the Earth's gravity is the dominating force. Because of this, many traditional satellite observation methods for detection and tracking are rendered unusable. Additionally, the current methods for imaging spacecrafts in LEO and GEO orbits are pushed to their limits from the difference in distance of cislunar objects being thousands of times further away. In nearer orbits, where we can rely on streaking stars to help identify spacecraft, at cislunar distances the objects typically are moving at speeds like that of the background stars relative to the observer. This makes visual detection of spacecraft virtually impossible.

With the growing number of lunar missions planned internationally, the necessity to understand how to handle observing this region of space becomes more important. The issues surrounding cislunar space are problems which have long since been identified but the competing priority of nearer orbits prevents these problems from being solved. As outlined in the *Center for Strategic and International Studies Aerospace Security Project* report from February 2022 [2], there are more than 30 cislunar missions planned within the next 5 years ranging from landing humans on the lunar surface for the first time in over 50 years to geographical surveying the Moon for future missions and lunar camps. To approach the issues surrounding cislunar space observations, we have successfully completed an imaging campaign using the recently launched James Webb Space Telescope (JWST) as our target of interest. This paper aims to outline the explored methods during our collection campaign including the application of techniques from other astronomy disciplines. Using ground-based optical sensors, we assess the quality of data products produced like images and photometric/astrometric results. This will provide insight into the challenges that are left to overcome before we are ready for continual XGEO observations using current systems.

Approved for Public Release; Distribution Unlimited. Public Release Case Number 22-2684

2. JAMES WEBB SPACE TELESCOPE MISSION OVERVIEW

The James Webb Space Telescope, NASA's next generation space telescope, has finally been deployed after over 25 years of development. The telescope specializes in the near-infrared spectrum and aims to explore the first light glow after the Big Bang, the very first galaxies to ever form, to examine the atmospheres of extrasolar planets, and more. The JWST launched out of the French Guiana on an Ariane 5 launch vehicle on December 25, 2021.

JWST's mission success relies on the cryogenic operating temperature for the electronics. Liquid cryogenic cooling techniques which were used for other space telescopes like the Spitzer Space Telescope cannot be scaled to JWST due to the size of the new telescope. Because of this, the JWST's orbiting location within the Sun-Earth L2 Lagrange point (Fig. 1.), where temperatures allow the James Webb to reach -370°F, was selected to help meet the cooling requirements. At Lagrange points, the gravitational pull of two large masses precisely equals the centripetal force required for a small object to move with them. [3].

The James Webb was selected for our target due to its convenient location in XGEO space as well as the unique opportunity for tracking and imaging the object as it travels through cislunar space to its destination. Since JWST is a public science mission, there is reliable information that we can access such as mission status and ephemerides. It is also an ideal target due to the size and reflectivity of the telescope's equipment.

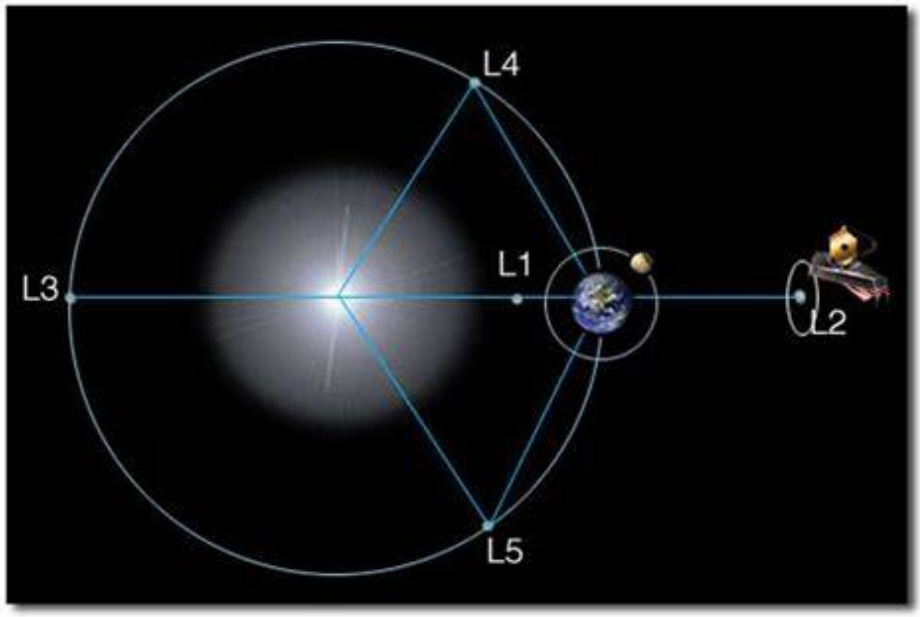

Fig. 1: Diagram showing the orbiting location of the James Webb Space Telescope in the Sun-Earth Lagrange point L2 [3]

3. METHODS

Due to the nature of XGEO space, common tracking methods are not valid since traditional tracking methods are not designed to handle the effects of the lunar and solar gravitational perturbations. Unlike targets in nearer orbits, where observers can use the streaking of background stars when tracking satellites to readily detect the target, XGEO distances are so great that the targets are moving at nearly the same rate as the background stars. This adds challenges to the detection of objects in cislunar space. Streaking stars are also used in the post-processing of satellite images which turns raw images into meaningful data products. This section will describe our way forward from these observation challenges.

Tracking

Traditional tracking of satellites is accomplished using a two-line element set encoding a list of orbital elements of an Earth-orbiting object for a given epoch (TLE) [4]. When objects are near the Moon, its gravitational effects cannot be ignored which renders the use of traditional Earth-orbiting Keplerian mechanics unusable. Currently, the best way to handle accurate position tracking of objects in XGEO is with ephemerides as the appropriate orbital perturbations from the moon can seamlessly be incorporated. Ephemerides are a table that provides the state (position and velocity vector components) of an object in the sky over each time step value [5]. Since the JWST is a NASA science mission, the ephemeris for the telescope is regularly updated every 2-3 weeks in the JPL Horizons ephemeris generation system [6]. Using the JPL Horizons system, ephemerides for JWST were generated and used for the telescope collection campaign.

Detection

For orbits closer to the Earth, visually detecting the object being tracked is straightforward. As a satellite is tracked, the telescope will follow the object at the same rate it is moving at (called rate track). This will in turn cause the background stars to streak by as the satellite stays stationary in frame as a point source. The further away the object is, the slower it moves relative to the observer and the smaller the background stars streak. For XGEO, the objects are so distant that they are moving nearly sidereal with visible changes in position only visible after tens of minutes. Visual detection of the object during imaging is crucial for ensuring the target is in frame and for validating the tracking accuracy of your system.

To address these challenges, we used a technique from the asteroid community who solely observes small distant objects. A common asteroid hunting method is by imaging the same region of the sky over some time then star-aligning the images using software. If the user "blinks" the star-aligned images in sequential order, anything moving in the field easily stands out in the images [7]. An example of this technique is shown in Fig. 2. below. A circle is drawn around the JWST and the images are numbered in sequential order. Using the grid as a reference, the James Webb is seen transiting left in the image frames as time passes between the images. The James Webb, which otherwise would be impossible to identify amongst background stars, becomes obvious in the images as it travels over the course of the night using this technique.

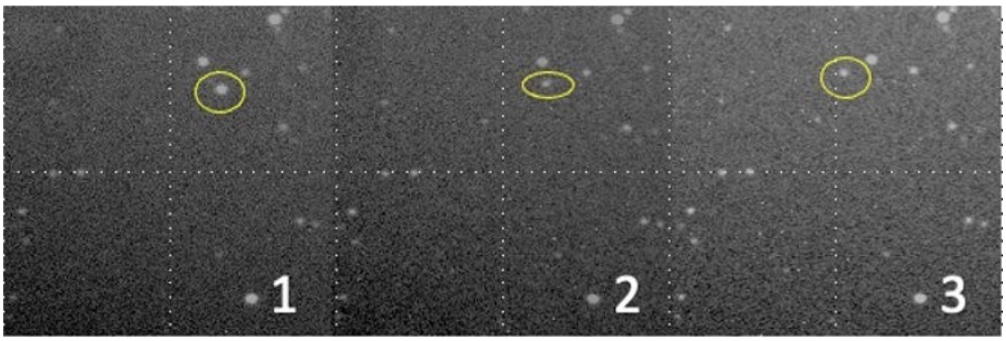

Fig. 2: The effects of the "blinking" technique regularly used by the asteroid community are shown. After star aligning the images and flipping through them in chronological order, any non-stellar objects that are otherwise impossible to locate are now obvious.

This process was done during the collection window to ensure the James Webb was being captured. Images were taken approximately every 10 minutes over the course of 1.5-2 hours. Once star-aligned and "blinked", the James Webb was revealed among the background stars.

Image Processing

We utilize custom image processing software to process FITS images of satellites into relevant data products like metric observations, pointing angles, and residuals. The software works by processing the images with Source Extractor software to first find the centroid of each star. The centroids are compiled into a binary table depicting the X, Y positions of the stars within the image FOV. Then, the binary table is sent through Astrometry.net software to register the X, Y positions to the star field in frame. The software then returns the Right Ascension (RA) and Declination

(DEC) position of the center of the image and plate model. Aberration correction is applied to the RA and DEC coordinate measurements before the orbit determination process.

The program typically uses a TLE catalog to complete the satellite correlation step of processing but without TLEs, an alternative method is required. The software was given a manual mode which allows a user to manually select the target in each image. However, this relies heavily on accurate visual detection of the object using the steps outlined above.

Telescope System Hardware and Software

Two observatory sites located in Colorado Springs, Colorado were used during the collection campaign. The first is Pine Park Engineering Corporation's Pine Park Observatory (PPO), which uses an 8" f/2 Celestron Rowe-Ackermann Schmidt Astrograph ("RASA") with a QHY-174M-GPS camera. The second site is the MITRE Observatory which uses an 11" f/10 Celestron EdgeHD Schmidt-Cassegrain telescope with a Finger Lakes Instrumentation Microline 50100 CCD camera.

Telescope control was accomplished using a custom telescope control program that interfaces with the telescope mounts. The program supports both rate-tracking and sidereal tracking modes which were used in parallel with JPL Horizon ephemerides to track the James Webb.

4. PHOTOMETRIC MEASUREMENTS AND TRACKING

Using the JPL Horizons tool to generate visibility predictions and ephemeris for tracking the JWST, both observatories were able to collect observations of the James Webb from December 27th, 2021 through January 13th, 2022. With the JPL Horizons predictions as well as the outlined methods, we were able to successfully collect over 2,100 observations of the James Webb over the course of its deployment to L2. Fig. 3 below shows an example of how the James Webb appeared in the images during the collection period. The James Webb moves so slowly relative to the sensor that the stars do not exhibit any streaking.

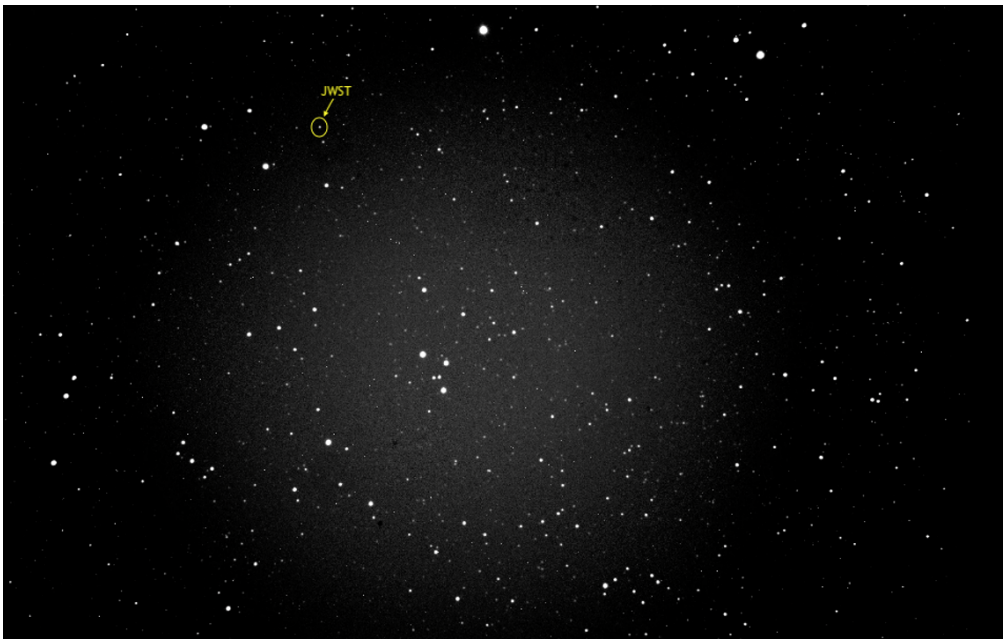

Fig. 3: Example image of the James Webb Space Telescope taken by the MITRE Observatory on January 5th, 2022. Arrow points to circle around JWST. The telescope was approximately 300,000 km from Earth at the time of this image.

We used custom image processing software to calculate the observed magnitude of the James Webb from the Pine Park Observatory. However, the photometry is not accurate and needs further calibration, so it only provides a rough

estimate of the magnitudes. Even with these magnitude estimates, we are able pull interesting pieces of information out of the data.

The mission status of the telescope is public information which allows us to correlate differences in the observed magnitude of the telescope to what deployment stage the James Webb was in [8]. Fig. 4 below shows this correlation. The first noticeable event where the observed magnitude began to increase took place at L+8 days which is when the telescope's sunshade covers began to be released. The second event was at L+14 days where the James Webb's primary mirror wings were deployed and latched together to begin forming the 6.5m aperture primary mirror. This resulted in another increase in the observed magnitude. The third traceable event was L+15.5 days through L+19 days where the primary mirror segments were aligned, and the primary mirror assembly was completed.

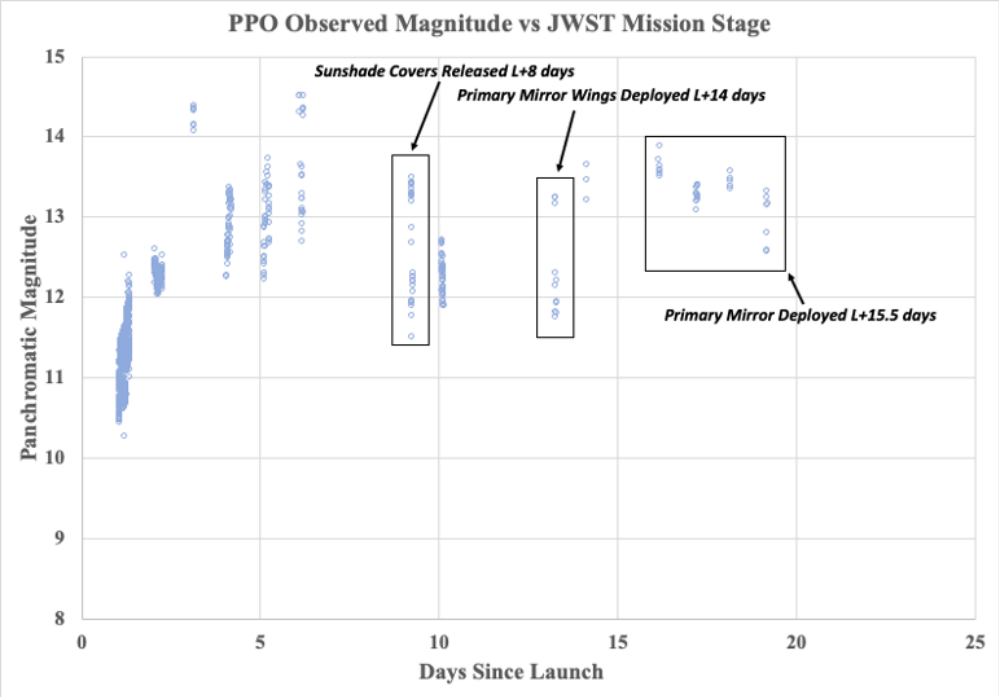

Fig. 4: Observed magnitude of the James Webb Space Telescope mapped to the different mission stages of its deployment.

Measurement errors in the observed RA and DEC position of the telescope were computed using the JPL Horizons ephemeris predictions as truth. These results are shown in Fig. 5. For both RA and DEC, the errors in the positions are minuscule. The ephemeris used for tracking provided high accuracy results even for an object in XGEO space and provide residuals that are in line with typical collection errors when using TLEs.

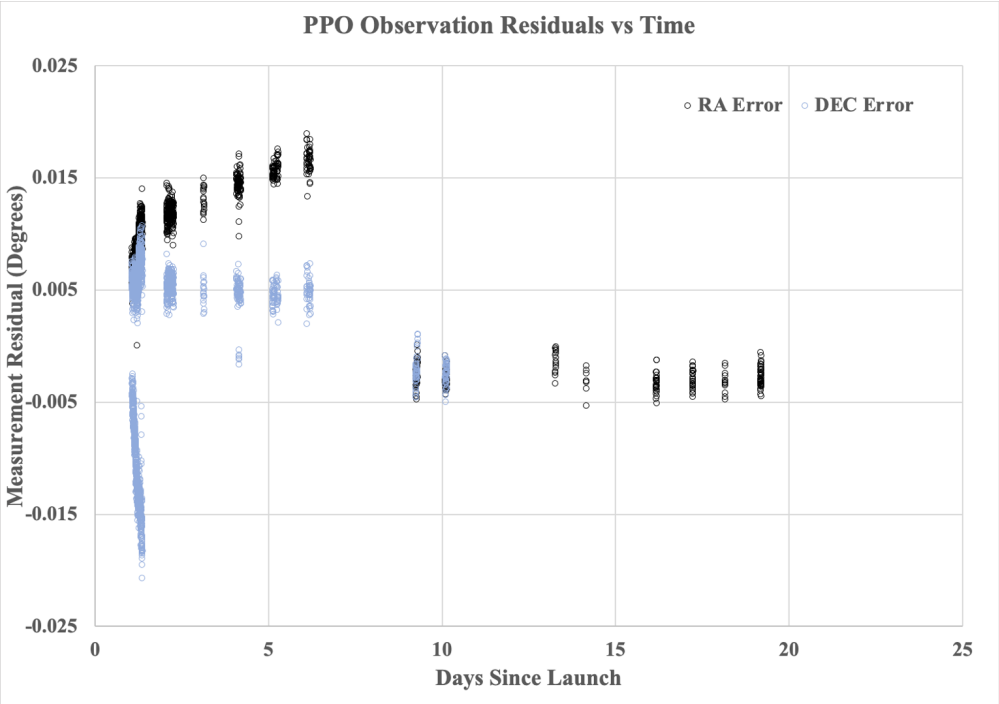

Fig. 5: Position measurement errors in RA and DEC of the James Webb Space Telescope observations over time as compared to JPL Horizons predictions.

Fig. 6 below shows the observed range measurements of the James Webb throughout its journey to L2 observed from PPO. Using the recorded values of the James Webb's predicted altitude from NASA [8], the observed range values from PPO are exactly what we expected.

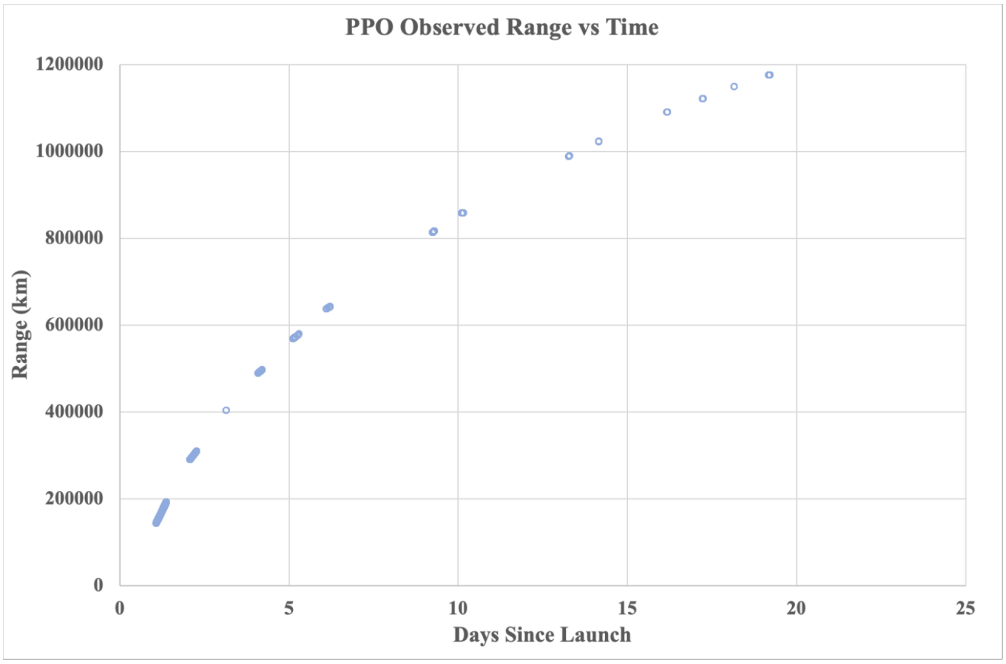

Fig. 6: Range measurements of the James Webb Space Telescope taken from Pine Park Observatory.

Additionally, the process we used for the James Webb collection works on multiple objects simultaneously. Fig. 7. below is the same position measurement residual plot as Fig. 5. but with the inclusion of a second object on L+1 days. This additional object is the rocket body that the telescope initially traveled in which was cross tagged in JPL Horizons ephemeris predictions. Since the predictions were based on the position of the telescope, we would expect the falling rocket body to have poor residuals as shown. These residuals can also be tracked to the rocket body separation event on L+1 days [8].

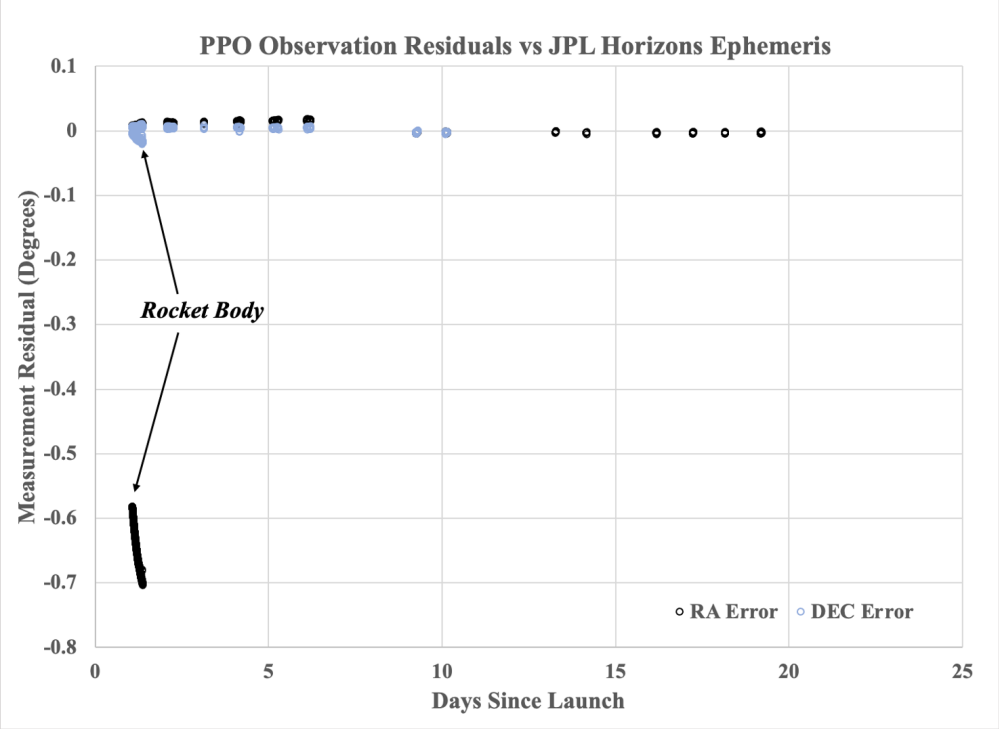

Fig. 7: Position measurement errors in RA and DEC of the James Webb Space Telescope observations over time as compared to JPL Horizons predictions. Large residuals were reported on L+1 days which was due to a second object being cross tagged with the JWST. This second object is the rocket body the telescope traveled in.

5. METRIC MEASUREMENTS

Using JWST predictions obtained from the JPL Horizons website for the Pine Park Observatory, PPO was able to track and collect photometric and metric data every night that the JWST was visible to PPO.

The previous section discussed the photometry and tied the brightness variations to en route events as the JWST headed to the Sun-Earth L2 Lagrange point. It showed that small, but high etendue telescopes can be valuable for tracking space objects in the cislunar orbital regime, to include XGEO and beyond.

Metric data reduction, as discussed in this section, illustrates that as space objects traverse from GEO (with typical geocentric distances near 6.6 Earth radii) to XGEO (with geocentric distances up to 66 Earth radii and beyond), orbit determination becomes much more difficult as the apparent points of light move little from night to night.

This section does metric data reduction for the earliest beyond-GEO track, obtained here in the western hemisphere on Christmas night 2021 (December 25, 2021, day 359). The observations themselves are time-tagged with December 26, day 360 UTC. This night's track started at 2021y 360d 01h 56m 49.173s and ended at 2021y 360d 08h 51m 50.603s (see Table 1).

The metric observations were thinned evenly to 366 observations to make the data reduction process much easier to manage and report.

Table 1 shows the PPO measurements for the 1st, 183rd (middle), and 366th (last) observations in this earliest tracking data set, also the JPL Horizons predictions for these same observations.

Table 1: PPO Observations vs. JPL Horizons Predictions.

Time, UTC yy ddd hh mm ss.sss	PPO RA hh mm ss.s	JPL RA hh mm ss.ss	PPO DEC ddd mm ss.ss	JPL DEC ddd mm ss.ss
21 360 01 56 49.173	05 20 26.8	05 20 19.94	-02 20 42.72	-02 22 33.70
21 360 05 21 49.881	05 22 53.8	05 22 50.38	-02 00 12.24	-02 01 48.20
21 360 08 51 50.603	05 24 02.6	05 24 04.59	-01 42 03.60	-01 44 06.40

Our initial approach to metric measurements reduction (i.e., orbit determination) with the 366 JWST observations was to use Gauss's method as given, for example, in [9], with the three observations given in Table 1, to find a preliminary two-body (Earth, JWST) solution.

However, we were able to improve on that solution using the **xGau** algorithm in Dr. Gim J. Der's *Astrodynamics Algorithms for Rapid Space Catalog Building* [10]. The improvement is that **xGau** does indeed provide the Gauss angles-only solution, but then goes on to account for the perturbations due to J2, J3, and most of J4, as per the Vint6 orbit propagation theory. The second column of Table 2 shows the **xGau** solution.

Next step in the orbit determination process is that we wanted a batch differential correction (DC) with all 366 observations, using the **xGau** solution to initiate the DC. For this we employed the **xBDC- optical-B3** algorithm in [9]. Given the **xGau** initial estimate, the **xBDC** algorithm converged in three iterations with a final RMS error of 3.884 arc-seconds. The results are shown in the third column of Table 2.

We should point out that the **xBDC- optical-B3** DC algorithm does not simply have two-body modeling. It has the following additional modeling: gravitational accelerations due to the WGS-84 12x12 geopotential [11] are accounted for, along with the gravitational accelerations due to the Moon and Sun, whose positions are modeled analytically.

Further, **xBDC-optical-B3** integrates the equations of motion numerically using the Runge-Kutta algorithm **rk711** as documented in [10].

Table 2: **xGau**, **xBDC-optical-B3**, and JPL Horizons Osculating Solutions.

Orbital Element	xGau Solution	xBDC-optical-B3 Solution	JPL Osculating Solution
Semi-major axis, $R_\oplus$	47.1141	76.1637	90.5798
Eccentricity	0.97708	0.98598	0.98819
Inclination, deg	4.12697	4.20944	4.24127
Rt. Asc. of Asc. Node, deg	88.4934	88.9826	88.9277
Arg. of Perigee, deg	190.526	192.193	192.329
Mean Anomaly, deg	18.4193	5.14848	5.96684
Mean Motion, rev/day	0.06066	0.02564	0.01977
Period, min	23738.7	56154.5	72836.2
Range at first observation, $R_\oplus$	22.6852	22.3521	22.9521
Range at 366th observation, $R_\oplus$	29.6072	29.7789	30.3015

We see good agreement between the **xGau** and **xBDC-optical-B3** algorithms with the JPL Horizons osculating solution exhibited in the fourth column of Table 2. How might the agreement be made better? **xBDC-optical-B3** already uses a special perturbations (SP) theory, Cowell's method, i.e., direct numerical integration of the equations of motion, rather than a general perturbations (GP) theory (e.g., Vint6 or SGP4).

Using JPL's DE405 solar, lunar, and planetary positions [12] for at least the Moon and Sun would provide results more in agreement with the numerically integrated JPL Horizons osculating solution. Also, including a solar radiation pressure model would help.

However, it should be kept in mind that although the JWST observation span was almost seven hours long (415 minutes), 415 / 72836 x 100 is only 0.570 per cent of the full orbital period of the almost-parabolic, osculating orbit that JWST was on during this leg of its journey to Sun-Earth L2. Given this, it is indeed remarkable that the PPO single-sensor solution came this close to the JPL Horizons osculating solution given in Table 2.

To sum up, we find that special perturbations modeling, i.e., Cowell's method (direct numerical integration of the equations of motion, to include at least the lunisolar gravitational accelerations and solar radiation pressure) is mandatory for accurate trajectory modeling in the cislunar/XGEO regimes. Cowell's method is the basis for the JPL Horizons predictions, and this is why we took the JPL Horizons predictions as our "truth model."

6. SUMMARY

This paper has documented the acquisition, detection, tracking, metric and photometric data collection, and data reduction for our observations of the James Webb Space Telescope through its deployment to Sun-Earth L2.

Using detection methods from other regions of astronomy, namely the asteroid community, we were able to modify our typical collection procedure to alleviate the issues surrounding object detection at lunar distances. Ephemeris generated by the JPL Horizons tool provided high accuracy tracking information which resulted in near zero position errors. These position residuals are also what we would expect when performing traditional satellite tracking on LEO or GEO objects with TLEs. Adding an option to our image processing tool to manually select the object in the images to bypass the lack of TLEs for object correlation allowed us to generate metric observations of the telescope. Furthermore, we successfully mapped events of the JWST's deployment to the observed telescope magnitude. The techniques used in this collection were not only able to track JWST in cislunar space, but multiple objects simultaneously as seen by the inclusion of the rocket body on the day after launch.

The IOD and DC results with the 366 observations used demonstrates some agreement between the JPL Horizons osculating solution and the two additional algorithms used for orbit determination, **xGau** and **xBDC-optical-B3**. Due to Moon and Sun gravitational perturbations not being accounted for in these methods, the Gauss, Laplace, HGM, and BDC IOD and DC results were not in-line with JPL predictions. Of the several methods tried, using Cowell's method to perform orbit prediction matched JPL predictions the best, which may be unsurprising given that JPL predictions are also based on Cowell's method.

The XGEO collection campaign on the James Webb Space Telescope was ultimately a success showing quality results in astrometric results with strong target tracking, detection, and processing results. If this process works on an object like the JWST on its journey to L2, it will work on any XGEO object given ephemeris can be generated.

REFERENCES

[1] Merriam-Webster. Cislunar. In *Merriam-Webster.com dictionary*. Retrieved May 2022, from `https://www.merriam-webster.com/dictionary/cislunar`

[2] K. Johnson. (2022). *Fly Me to The Moon Worldwise Cislunar and Lunar Missions*, Center for Strategic International Studies Aerospace Security Report.

[3] NASA. *Webb Orbit*. Retrieved June 2022, from `https://webb.nasa.gov/content/about/orbit.html`

[4] Wikipedia. Two-line element set. In *Wikipedia*. Retrieved June 2022, from `https://en.wikipedia.org/w/index.php?title=Two-line_element_set&oldid=1104028347`

[5] Wikipedia. Ephemeris. In *Wikipedia*. Retrieved June 2022, from `https://en.wikipedia.org/w/index.php?title=Ephemeris&oldid=1093513166`

[6] NASA. *Moving Target Ephemerides - JWST User Documentation*. Retrieved June 2022, from `https://jwst-docs.stsci.edu/methods-and-roadmaps/jwst-moving-target-observations/jwst-moving-target-supporting-technical-information/moving-target-ephemerides`

[7] Sky and Telescope. *Hunting Asteroids From Your Backyard*. Retrieved May 2022, from `https://skyandtelescope.org/observing/celestial-objects-to-watch/hunting-asteroids-from-your-backyard/`

[8] NASA. *James Webb Space Telescope Deployment Explorer*. Retrieved June 2022, from `https://jwst.nasa.gov/content/webbLaunch/deploymentExplorer.html`

[9] H. D. Curtis, *Orbital Mechanics for Engineering Students*, Elsevier, Second Edition, 2009.

[10] G. J. Der, *Astrodynamics Algorithms for Rapid Space Catalog Building*, Der Astrodynamics (2021), Dallas, Texas. Retrieved June 2022, from: `https://derastro.com`

[11] Defense Mapping Agency WGS-84 Development Committee, *Department of Defense World Geodetic System 1984 – Its Definition and Relationships with Local Geodetic Systems*, DMA Technical Report 8350.2 (30 Septem-

ber 1987).
[12] JPL's DE405 and DE406 are available from Willmann-Bell on CD-ROM. Retrieved June 2022, from: https://shopatsky.com/collections/willmann-bell

The author's affiliation with The MITRE Corporation is provided for identification purposes only, and is not intended to convey or imply MITRE's concurrence with, or support for, the positions, opinions, or viewpoints expressed by the author.'